Catalysis Today xxx (2014) xxx–xxx

Contents lists available at ScienceDirect

Catalysis Today

journal homepage: www.elsevier.com/locate/cattod

Can surface energy measurements predict the impact of catalyst hydrophobicity upon fatty acid esterification over sulfonic acid functionalised periodic mesoporous organosilicas?

Cyril Pirez[a,b], Adam F. Lee[c], Christopher Jones[a], Karen Wilson[c,*]

[a] School of Chemistry, Cardiff University, Park Place, Cardiff CF10 3AT, UK
[b] UCCS, University of Lille I, 59655 Villeneuve d'Ascq, France
[c] European Bioenergy Research Institute, School of Engineering and Applied Sciences, Aston University, Birmingham B4 7ET, UK

ARTICLE INFO

Article history:
Received 14 November 2013
Received in revised form 19 January 2014
Accepted 27 January 2014
Available online xxx

Keywords:
Solid acid
Free fatty acid esterification
Periodic mesoporous organic materials
Inverse gas chromatography
Hydrophobicity
Biodiesel

ABSTRACT

Sulfonic acid functionalised periodic mesoporous organosilicas ($PrSO_3H$-PMOs) with tunable hydrophobicity were synthesised via a surfactant-templating route, and characterised by porosimetry, TEM, XRD, XPS, inverse gas chromatography (IGC) and ammonia pulse chemisorption. IGC reveals that incorporation of ethyl or benzyl moieties into a mesoporous SBA-15 silica framework significantly increases the non-specific dispersive surface energy of adsorption for alkane adsorption, while decreasing the free energy of adsorption of methanol, reflecting increased surface hydrophobicity. The non-specific dispersive surface energy of adsorption of PMO-SO_3H materials is strongly correlated with their activity towards palmitic acid esterification with methanol, demonstrating the power of IGC as an analytical tool for identifying promising solid acid catalysts for the esterification of free fatty acids. A new parameter $\left[-\Delta G^{C}_{NP-P}\right]$, defined as the per carbon difference in Gibbs free energy of adsorption between alkane and polar probe molecules, provides a simple predictor of surface hydrophobicity and corresponding catalyst activity in fatty acid esterification.

1. Introduction

The production of second-generation biofuels and platform chemicals derived from renewable non-food feedstocks such as lignocellulosic or algal biomass, and agricultural waste such as corn husks and wood chippings, offers improved sustainability over current petroleum derived energy and chemical sources [1]. The conversion of bio-based molecules (e.g. sugars, triglycerides, fatty acids or other platform molecules) often involves reactions with highly polar molecules whose transformations liberate H_2O via condensation or dehydration pathways. Biodiesel produced from non-edible plant, algal or waste oil sources is one such commercially available advanced biofuel wherein water content can have a detrimental effect on productivity [2]. Biodiesel synthesis commonly involves the homogeneously base or acid catalysed transesterification/esterification of triglyceride (TAG) and fatty acid (FFA) bio-oil components by short-chain alcohols to the respective fatty acid methyl ester (FAME). While such soluble alkali base catalysed biodiesel processes are extremely rapid, their high sensitivity to water (which hydrolyses triglycerides to FFAs) makes them ill-suited to bio-oils containing significant FFA components, with associated undesired soap formation and attendant separation issues [3,4]. Commercial biodiesel manufacture employs catalytic pre-esterification of the bio-oil feedstock to convert free fatty acids to their corresponding esters in order to circumvent these problems; however water sensitivity remains an issue. Consequently, there is much interest in the application of mesoporous solid acids in biodiesel synthesis [5], with sulfonated silicas [6–12] and polymers [13–17], polyoxometallates [18–20], mixed oxides [17,21,22] and sulfated oxides [17,23–26] amongst others explored for FFA esterification with methanol. Although high activities are achievable under mild conditions, delivering high ester yields is challenging, particularly at elevated water contents [27].

Surface functionalisation of sulfonic acid silicas with inert, apolar octyl groups can enhance the FFA esterification by increasing acid strength and surface hydrophobicity [10]. While promising, optimising catalyst performance via simple alkyl grafting routes is restricted by the availability of tethering sites on the silica surface. In contrast, periodic mesoporous organosilicas (PMOs) are an interesting class of materials prepared via the co-condensation of $Si(OEt)_4$ with different bridged organo-silane precursors to create ordered mesoporous silicas incorporating organic functions directly into the silica walls [28–30]. Such hybrid organic–inorganic porous solids offer exciting applications across

* Corresponding author. Tel.: +44 121 204 5456.
E-mail address: k.wilson@aston.ac.uk (K. Wilson).

0920-5861/$ – see front matter © 2014 Elsevier B.V. All rights reserved.
http://dx.doi.org/10.1016/j.cattod.2014.01.042

materials science, and to date PMOs possessing organic bridging $(RO)_3$–Si–$(OR)_3$ units with methylene [31–33], ethylene [29,33,34], ethylidene [28,35–37], phenylene [33,38–42], biphenylene [43,44], thiophene [42,45,46] and anthracene [47–49] substituents have been reported. Ethyl and phenyl organic linkers are the most widely studied in catalysis because they afford a more homogeneous distribution of organic moieties, and improved surface crystallinity and thermal stability [38,39]. The utility of such materials in catalysis is of particular interest as the inclusion of different organic moieties within the framework offers a unique opportunity to tune surface polarity and hydrophobicity; critical parameters in controlling adsorption, reactant activation and product selectivity in liquid and vapour phase catalysis.

The development of next generation catalysts for biomass conversion requires improved methods to quantify the impact of surface hydrophobicity upon adsorption phenomena and the kinetics of liquid phase catalytic reactions [50,51]. The hydrophobic properties of porous materials are often empirically defined, hampering our ability to tailor catalyst surfaces in an informed manner. Simple contact angle measurements are ill-suited to the analysis of powdered solids [52] since particle morphology/porosity can influence the shape of probe droplets and their absorption. Inverse gas chromatography (IGC) is a powerful but under-utilised technique for characterising catalysts, allowing surface–adsorbate interactions to be investigated over porous catalysts, and thermodynamic properties including surface tension, acid/base character and heats of adsorption to be determined. IGC is often employed to characterise polymers or glassy materials [53] and pharmaceutical samples, and has been used to study the adsorption properties of carbonaceous materials [54,55], zeolites [56–58], and amorphous [59,60] and templated silicas [61]. In respect of catalysis, IGC has been exploited to correlate reactivity with the adsorption of specific reactants in propene partial oxidation over Pd [62], CO oxidation over Pt and Rh [63], VOC combustion over Mn–Zr mixed oxides [64], and benzene benzylation over Fe–ZSM-5 [65], however, there are no previous reports applying IGC to correlate catalyst hydrophobicity and associated activity.

Here we report the application of IGC to extract a new parameter for quantifying the hydrophobic properties of mesoporous catalysts which correlates with their turnover frequency (TOF) in palmitic acid esterification by methanol; a prototypical reaction pertinent to biodiesel production wherein high local concentrations of reactively-formed H_2O can impede the forward reaction pathway to the desired fatty acid methyl esters [66].

2. Experimental

2.1. Chemicals

Mercaptopropyl trimethoxysilane (MPTS, Alfa Aesar 95%); toluene (Fisher 99%); TEOS (tetraethoxyorthosilane, Aldrich 99%); HCl (Fisher 36 wt%); methanol (Fisher 99%); hydrogen peroxide (Sigma-Aldrich 30 vol%); hexanoic acid (Aldrich 99%); palmitic acid (Aldrich 99%); 1.4-bis(triethoxysilyl)benzene (BTSB, Aldrich 96%); 1.2-bis(triethoxysilyl)ethane (BTSE, Aldrich 96%); ammonia (BOC, 99.98%).

2.2. Synthesis of SBA-15 and PMO materials

Periodic mesoporous organosilicas with 0%, 25% and 50% ethyl/phenyl hybridisation were synthesised following the protocol of Sanchez-Vazquez et al. [67]. Briefly, 3 g of Pluronic P123 triblock copolymer was dissolved in 112 cm^3 of water and 1 cm^3 of HCl under stirring at 40 °C. The appropriate mixture of TEOS and BTSE (BTSB) precursor required to achieve the desired degree of hybridisation was subsequently added to the surfactant solution (Table 1), and stirred at 40 °C for a further 72 h. The mixture was then aged at 130 °C for 24 h and the resulting solid product filtered, washed three times with deionised water and dried at room temperature. Residual P123 template was extracted via a 24 h reflux with EtOH/1 M HCl solution and filtered and dried to afford the final powdered PMO support.

Table 1
Stoichiometry of reactant mixtures employed in PMO synthesis.

Nominal organic hybridisation (mol%)	Molar composition				
	TEOS	BTSE (BTSB)	P123	HCl	H_2O
SBA-15	0.0414	0	0.00069	0.0159	8
25% BTSE (E25)	0.031	0.0052	0.00069	0.0159	8
50% BTSE (E50)	0.0207	0.0103	0.00069	0.0159	8
25% BTSB (B25)	0.031	0.0052	0.00069	0.0159	8
50% BTSB (B50)	0.0207	0.0103	0.00069	0.0159	8

2.3. Sulfonic acid grafting

PMO materials were subsequently sulfonic acid functionalised via a grafting route in which 1 g of each material was added to a solution containing 1 cm^3 of MPTS in 30 cm^3 of toluene. The resulting suspension was refluxed at 130 °C under stirring for 24 h, and the thiol-functionalised solid then filtered, washed 3 times with methanol and dried at 80 °C overnight. Thiol groups were oxidised to $-SO_3H$ by mild oxidation with 30 cm^3 of 30 vol% H_2O_2 through continuous stirring of the thiolated PMO at room temperature for 24 h. The sulfonated product was filtered, washed three times with methanol and dried at 80 °C, and the final $PrSO_3H$-PMO stored in air and used without further treatment.

2.4. Characterisation

Nitrogen physisorption was undertaken on a Quantachrome Nova 2000e porosimeter using NOVAWin software. Samples were degassed at 120 °C for 2 h prior to analysis by N_2 adsorption at −196 °C. BET surface areas were calculated over the relative pressure range 0.01–0.2. Pore diameters and volumes were calculated applying the BJH method to the desorption isotherm for relative pressures >0.35. Low angle powder XRD patterns were recorded on a PANalytical X'pertPro diffractometer fitted with an X'celerator detector and Cu K_α (1.54 Å) source calibrated against a Si standard (PANalytical). Low angle patterns were recorded for $2\theta = 0.3–8°$ with a step size of 0.01°. TEM micrographs were obtained with a Phillips CM12 transmission electron microscope operated at 100 kV, with images recorded by a SIS MegaView III digital camera. Image analysis was undertaken using ImageJ software. XPS was performed on a Kratos Axis HSi X-ray photoelectron spectrometer fitted with a charge neutraliser and magnetic focusing lens employing Al K_α monochromated radiation (1486.6 eV). Spectral fitting was conducted using CasaXPS version 2.3.14, with binding energies corrected to the C 1s peak at 284.8 eV and S 2p XP spectra fitted using a common Gaussian/Lorentzian peak shape. Errors were estimated by varying the Shirley background subtraction procedure across reasonable limits and re-calculating fits. TGA was performed using a Stanton Redcroft STA780 thermal analyser on ~10–20 mg samples under a 10 vol% O_2/He mixtures (20 cm^3 min^{-1} total flow) during heating at 20 °C min^{-1} in order to study the decomposition of organic moieties. Surface energies at infinite dilution were determined by a fully-automated Surface Measurement Systems Ltd inverse GC system. Samples were outgassed for 2 h at 120 °C to remove physisorbed water and impurities on the surface prior to exposure to ethyl acetate, methanol or alkane pulses. Full details of the experimental procedure are given in the ESI. Surface properties

Please cite this article in press as: C. Pirez, et al., Can surface energy measurements predict the impact of catalyst hydrophobicity upon fatty acid esterification over sulfonic acid functionalised periodic mesoporous organosilicas? Catal. Today (2014), http://dx.doi.org/10.1016/j.cattod.2014.01.042

were determined according to literature methods [68,69]. Surface acidity was measured via NH_3 pulse chemisorption and on-stream MS detection. Briefly, 50 mg of sample was outgassed at 120 °C for 2 h and then cooled to 100 °C. Consecutive injections of 100 μl NH_3 were passed over samples and the resulting eluted ammonia quantified until the signal saturated.

2.5. Catalytic esterification

Reactions were performed using a Radleys Carousel Reactor Station at atmospheric pressure. 12.5 cm^3 (300 mmol) or methanol, 10 mmol of hexanoic (C6) or palmitic (C16) acid, and 2.5 mmol of hexylether (as an internal standard) were added to a sealed glass reactor tube under stirring at 60 °C. 0.05 g of sulfonic acid catalyst was subsequently introduced, and aliquots of the reaction mixture periodically withdrawn and filtered and diluted with dichloromethane for analysis on a Varian 450-GC. Analysis of reaction products from palmitic acid esterification employed a 1079 programmable, direct on-column injector and Phenomenex ZB-1HT Inferno 15 m × 0.53 mm × 0.15 μm capillary column. Initial rates were calculated over the first two hours of reaction, wherein similar acid conversions of 5–10% were obtained, so as to be in a regime where the concentrations of reactively-formed water were comparable. Product yields determined from response factors for methyl palmitate, with mass balances determined to be >98%. Errors in TOF were calculated from the variance in the line of best fit to initial rate plots, and repeat measurements of initial rate and acid site titrations on selected catalysts, from which a composite error of ±5% was determined.

3. Results and discussion

The successful synthesis of ethyl and phenyl derivatised PMOs (E25, E50, B25 and B50) was first assessed by detailed bulk and surface characterisation to confirm the existence of ordered mesoporous structures and quantify the degree of organic incorporation prior to sulfonation (Figs. S1–5). Porosimetry of the as-prepared PMO materials confirmed that they all exhibit type IV isotherms similar to that of SBA-15 mesoporous silica. Corresponding pore size distributions show only a slight contraction in the BJH mean mesopore diameter of the PMOs (5–8–6.7 nm) compared with SBA-15 (7 nm), with the smallest pores associated with incorporation of bulky phenyl bridges or a high concentration of ethyl bridges. Since these pore contractions are small, they are unlikely to induce significant differences in mass-transport for the PMOs with respect to SBA-15. The latter is important if the impact of organic framework modification of SBA-15 upon reactivity is to be isolated from any potential textural variations (which can strongly influence esterification as reported for SBA-15-Pr-SO_3H versus KIT-6-Pr-SO_3H catalysts [11,12]). Likewise, BET surface areas were all comparable to pure SBA-15 decreasing only from 850 to 757 $m^2\,g^{-1}$ for the highest loading B50 sample (Table S1). Low angle XRD patterns evidenced common peaks for SBA-15 and all PMOs, attributable to the 100, 110 and 200 reflections characteristic of *p6mm* hexagonal close-packed architectures [70], showing that the parent SBA-15 structure is retained even following the incorporation of 50 mol% organic bridges into the silica framework. TEM likewise confirms that all four PMOs possess well-ordered mesopore networks with the same micron-long parallel channels and hexagonal architectures observed for SBA-15. Although the unit cell of SBA-15 and all four PMOs are essentially identical, wall thickness expands with increasing organic hybridisation as expected upon substitution of siloxane with ethyl/phenyl silyl linkers (Table S1), indicative of a mechanically robust material. Temperature programmed oxidation was used to quantify the organic content of

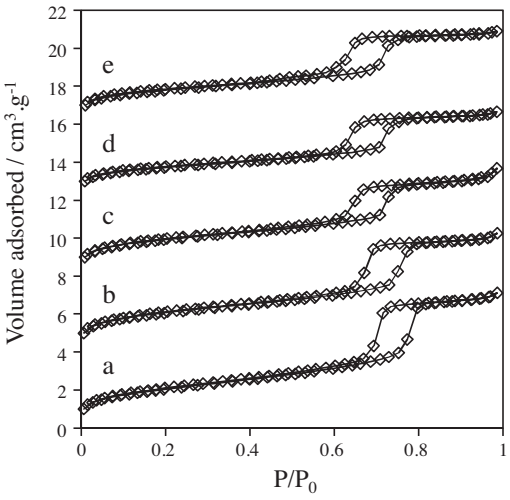

Fig. 1. Nitrogen adsorption–desorption isotherms of sulfonic acid grafted SBA-15 and PMOs; (a) $PrSO_3H$-SBA-15, (b) $PrSO_3H$-E25, (c) $PrSO_3H$-E50, (d) $PrSO_3H$-B25, (e) $PrSO_3H$-B50. (Note—isotherms offset for clarity).

the PMO materials (Fig. S5), and hence degree of hybridisation, from the fractional mass loss occurring between 300–400 °C (E25/E50) and 600–800 °C (B25/B50). SBA-15 exhibits negligible change over this temperature regime, whereas the PMOs display significant high temperature mass losses, which increase from ~3 to 13 wt% across the series with the degree of hybridisation and carbon content of the BTSE or BTSB precursor (Table S1).

Structural and textural properties of the parent SBA-15 and PMOs are preserved after sulphonic acid derivatisation via MPTS grafting and oxidation; porosimetry shows the retention of type IV isotherms (Fig. 1), while XRD (Fig. 2) and TEM (Fig. 3) showed the expected *p6mm* hexagonal close-packed architecture. Surface areas, pore volumes and mesopore diameters only decrease slightly as expected due to the introduction of in-pore sulfonic groups (Table 2).

The sulphur content, acid site loadings and densities of $PrSO_3H$–PMOs are summarised in Table 3 and decrease with increasing BTSE and BTSB incorporation. This is attributed to decreased availability of siloxane groups for grafting of MPTS as the degree of organic hybridisation is increased. MPTS grafting was performed in toluene in order to ensure consistency with our previous work, however it should be noted that these conditions give rise to

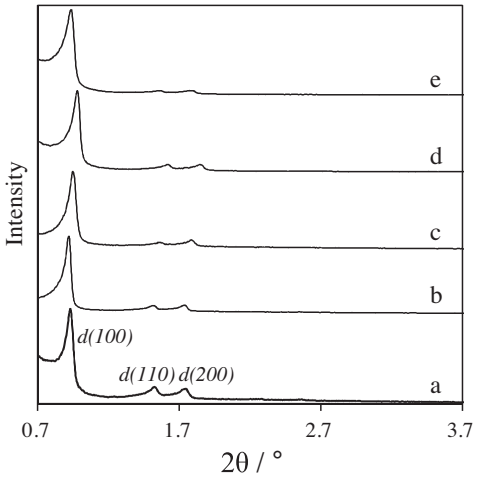

Fig. 2. XRD patterns of sulfonic acid grafted SBA-15 and PMOs; (a) $PrSO_3H$-SBA-15, (b) $PrSO_3H$-E25, (c) $PrSO_3H$-E50, (d) $PrSO_3H$-B25, (e) $PrSO_3H$-B50.

Please cite this article in press as: C. Pirez, et al., Can surface energy measurements predict the impact of catalyst hydrophobicity upon fatty acid esterification over sulfonic acid functionalised periodic mesoporous organosilicas? Catal. Today (2014), http://dx.doi.org/10.1016/j.cattod.2014.01.042

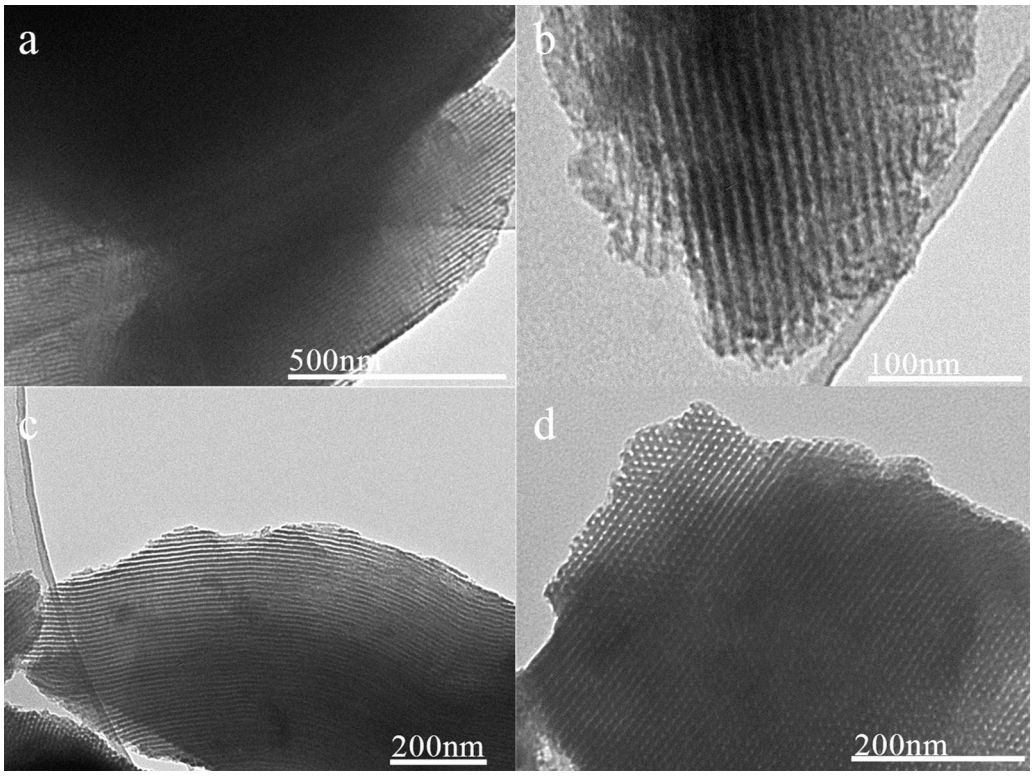

Fig. 3. TEM picture of sulfonic acid grafted PMOs; (a) $PrSO_3H$-E25, (b) $PrSO_3H$-E50, (c) $PrSO_3H$-B25, (d) $PrSO_3H$-B50.

Table 2
Summary of textural and structural properties for Pr-SO_3H/PMO materials.

Catalyst	BET ($m^2\ g^{-1}$)	V_p ($cm^3\ g^{-1}$)	W_{BJH} (nm)	Plane spacing (nm)	Unit cell parameter (nm)	Wall thickness (nm)	Framework organic content[a] (wt%)
Pr-SO_3H-SBA-15	800	1.34	7.2	9.5	11	3.8	<1
Pr-SO_3H-E25	825	1.2	6.7	9.6	11.1	4.4	3
Pr-SO_3H-E50	760	1.07	5.8	9.3	10.8	5	4.1
Pr-SO_3H-B25	746	1.14	5.8	9	10.4	4.6	10
Pr-SO_3H-B50	698	0.82	5.8	9.4	10.9	5	13.3

[a] Mass loss observed between 300 and 400 °C (BTSE) or 600 and 800 °C (BTSB) during temperature-programmed oxidation on parent PMO material prior to sulfonic acid derivatisation.

lower loadings of grafted species [71,72] since competitive toluene adsorption at organic domains hinders thiol access to neighbouring silanol groups during grafting [73].

Having verified that the organic content of our $PrSO_3H$-PMOs could be readily varied, IGC at infinite dilution was subsequently applied to explore their surface energies and associated hydrophobicity. The surface energy of an adsorbent $\left(\gamma^S\right)$ is given by the sum of dispersive $\left(\gamma_D^S\right)$ and specific free energy $\left(\gamma_{SP}^S\right)$ components according to Eq. (1):

$$\gamma^S = \gamma_D^S + \gamma_{SP}^S \tag{1}$$

The standard free energy of adsorption ΔG_{ads} is likewise determined by the dispersive and specific energies for adsorption according to Eqs. (2) and (3) [74], wherein V_N is the specific retention volume of the adsorbate:

$$[-\Delta G_{ads}] = \left[-\Delta G_{ads}^D\right] + \left[-\Delta G_{ads}^{SP}\right] \tag{2}$$

$$\Delta G_{ads} = -RT \times \ln V_N + \text{constant} \tag{3}$$

Non-polar molecules adsorb via non-specific, attractive London forces, whereas the adsorption of polar molecules also includes specific contributions arising from e.g. acid/base, hydrogen and

Table 3
Surface composition, acid site loading and IGC parameters for $PrSO_3H$-PMOs and $PrSO_3H$/SBA-15.

Catalyst	Surface composition and acidity				IGC measurements[a,b]	
	Surface S content (wt%)	Surface C:Si atomic ratio	Acid site loading $\left(mmol_{H^+}\ g^{-1}\right)$	Acid site density ($H^+\ nm^{-2}$)	γ_D^S ($mJ\ m^{-2}$)	$-\Delta G_{ads}^{SP}$ (MeOH) ($kJ\ mol^{-1}$)
$PrSO_3H$-SBA-15	0.26	0.18	0.2	0.15	34.1	22.2
$PrSO_3H$-E25	0.60	0.55	0.07	0.05	47.8	30.8
$PrSO_3H$-E50	0.47	0.83	0.05	0.04	64.5	18.9
$PrSO_3H$-B25	0.5	0.91	0.06	0.05	70.8	20.5
$PrSO_3H$-B50	0.28	2.58	0.03	0.03	72.3	18.0

[a] Dispersive energy and specific free energy measured from the extracted materials prior to derivatisation with sulfonic acid groups.
[b] For alkanes it is assumed that $\gamma_{SP}^S = 0$ and hence $\gamma^S = \gamma_{SP}^S$.

Please cite this article in press as: C. Pirez, et al., Can surface energy measurements predict the impact of catalyst hydrophobicity upon fatty acid esterification over sulfonic acid functionalised periodic mesoporous organosilicas? Catal. Today (2014), http://dx.doi.org/10.1016/j.cattod.2014.01.042

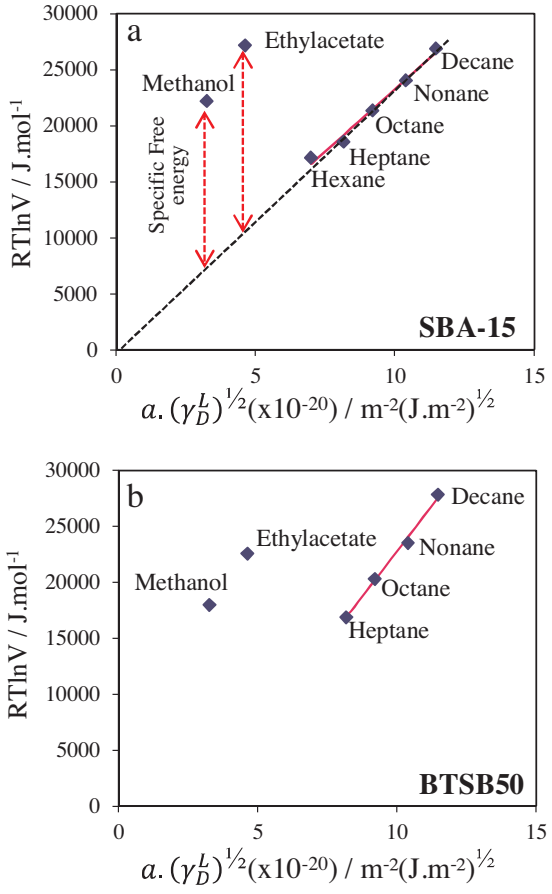

Fig. 4. IGC plot for (a) SBA-15 and (b) B50 showing the general method for determining γ_D^S and $-\Delta G_{ads}^{SP}$.

π-bonding interactions with the surface. Dispersive surface energies (γ_D), which are related to non-specific Van der Waals interactions, can be obtained by studying the adsorption of a homologous series of e.g. C_6 to C_{10} alkane probe molecules onto each $PrSO_3H$-PMO sample. A linear relationship is predicted between $RT \times \ln\left(V_N^{alkane}\right)$ and the dispersive components of surface energies for the adsorbent and probe molecules γ_D^S and γ_D^L, respectively, according to Eq. (4) [75], where N is Avogadro's number, a is the surface area of the probe molecule, and γ_N^{alkane} the specific retention volume of an alkane with N carbon atoms which in turn is proportional to its specific retention time as measured by IGC:

$$RT \times \ln\left(V_N^{alkane}\right) = 2N \times a \times \left(\gamma_D^S\right)^{1/2} \times \left(\gamma_D^L\right)^{1/2} + \text{constant} \quad (4)$$

A plot of $RT \times \ln\left(V_N^{alkane}\right)$ against $a \times \left(\gamma_D^L\right)^{1/2}$ should yield a straight line with slope $2N \times a \times \left(\gamma_D^S\right)^{1/2}$, as observed in Fig. 4. Measurement of the retention time (volume) for a series of alkane adsorbates thus enables determination of the non-specific dispersive component of the surface energy $\left(\gamma_D^S\right)$ across our family of $PrSO_3H$-PMO adsorbents [76]. Extrapolating horizontally from the resulting gradient yields an intersect with the ordinate indicative of the non-specific, dispersive component of the adsorption energy $\left(-\Delta G_{ads}^{SP}\right)$. The same procedure can be adopted for polar probe molecules with acid, base or amphoteric character by similarly measuring their retention time (volume) and calculating RTlnV which is proportional to their total free energies of adsorption $-\Delta G_{ads}$.

Table 4
Performance of $PrSO_3H$-SBA-15 and $PrSO_3H$-PMO catalysts in palmitic acid esterification with methanol.

Catalyst	Palmitic acid conversion[a](%)	Palmitic acid TON[a]	Initial rate[b] (mmol h^{-1})	TOF[c,d] (h^{-1})
Pr-SO_3H/SBA-15	55	540	0.4046	41
Pr-SO_3H/E25	47	1338	0.2983	85
Pr-SO_3H/E50	46	1702	0.2995	111
Pr-SO_3H/B25	49	1570	0.3138	95
Pr-SO_3H/B50	38	2441	0.1836	118

[a] After 24 h reaction.
[b] Initial rate calculated from ester yield after 2 h reaction.
[c] TOF calculated from initial rate $mmol_{H^+}$ (obtained from NH_3 pulse titration).
[d] Catalyst leaching to validate these calculations was verified by hot filtration tests (Fig. S9) which showed no residual activity after catalyst removal, and sulfur analysis of spent catalysts which showed only a small (<5%) decrease in S content post-reaction, confirming catalyst stability under these mild reaction conditions.

Fig. 4 shows a representative plot of such surface energy calculations for SBA-15 and B50 using methanol and ethyl acetate as the polar probe molecules. The free energy of adsorption $-\Delta G_{ads}$ for polar probes lies above the extrapolated line arising from the homologous alkane series (whose adsorption is dominated by non-specific dispersive interactions). This extrapolation enables $-\Delta G_{ads}^{D}$ for a hypothetical *n*-alkane having the same saturated vapour pressure [77] and number of carbon atoms as the polar probe. According to Eq. (3), the difference between these free energies gives the specific free energy for adsorption of that polar molecule $\left(-\Delta G_{ads}^{SP}\right)$. Similar plots for the other PMO materials are shown in Fig. S4. Table 3 summarises the resulting non-specific surface energies γ_D^S and specific free energies of methanol adsorption $-\Delta G_{ads}^{SP}$ (MeOH).

The data in Table 3 shows that the non-specific dispersive energy γ_D^S for the PMO surfaces increases with the degree of organic functionalisation of support walls, following the order E25 < E50 and B25 < B50. Phenyl groups within the silica framework increases the strength of alkane adsorption relative to ethyl functionalised silica. This increased organophilicity can be rationalised in terms of the number of CH_x groups per phenyl versus ethyl unit, and is in accordance with the overall organic content reported in Table 2. Trends in the corresponding $-\Delta G_{ads}^{SP}$ (MeOH) for the PMOs show a contrasting decrease with increasing organic character, suggesting that methanol binding to surface Si–OH and Si–O–Si [78] moieties is significantly weakened.

Palmitic acid esterification with methanol was subsequently investigated to explore the impact of $PrSO_3H$-PMO surface properties upon their corresponding activity (Fig. S7 and Table 4). All $PrSO_3H$-PMOs solid acids show promising initial rates, which are ~25–50% lower than the benchmark $PrSO_3H$-SBA-15 catalyst despite the latter possessing 65–85% more acid sites. Consequently, the acid site normalised turnover number (TON) thus increases systematically with framework organic content (Fig. S8). Turnover frequencies (TOFs) (calculated from initial rates at comparable conversion levels to ensure similar concentrations of reactively formed water), were likewise found to increase monotonically with framework organic content (Table 4).

Fig. 5 compares the trends in palmitic acid esterification TOF, non-specific dispersive surface energy $\left(\gamma_S^D\right)$, and $-\Delta G_{ads}^{SP}$ (MeOH) across the PMO series. The rise in γ_S^D is mirrored by that in catalytic esterification activity, precisely as $-\Delta G_{ads}^{SP}$ (MeOH) decreases. Since γ_S^D reflects non-specific adsorbate interactions, it provides a measure of the surface affinity for alkyl chains such as integral to FFAs (lipophilicity). In contrast $-\Delta G_{ads}^{SP}$ (MeOH) provides a measure of surface hydrophilicity and hence unsurprisingly displays the reverse behaviour.

It is interesting to note that the relative changes in TOF and γ_s appear to show some non-linearity on going from 4.1 to 10 wt%

Please cite this article in press as: C. Pirez, et al., Can surface energy measurements predict the impact of catalyst hydrophobicity upon fatty acid esterification over sulfonic acid functionalised periodic mesoporous organosilicas? Catal. Today (2014), http://dx.doi.org/10.1016/j.cattod.2014.01.042

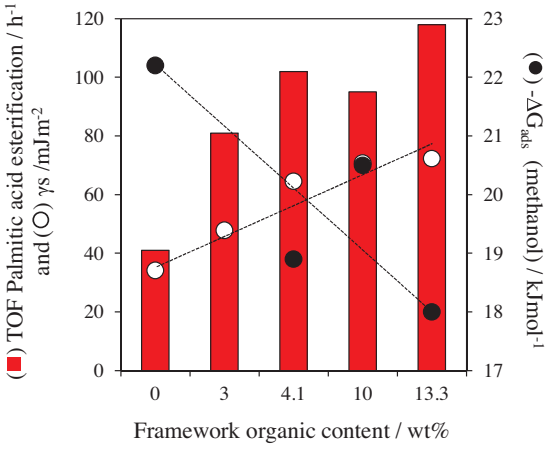

Fig. 5. Impact of framework organic content on PMO surface properties (non-specific dispersive energy and free energy for methanol adsorption) as determined from IGC and TOF for palmitic acid esterification with methanol.

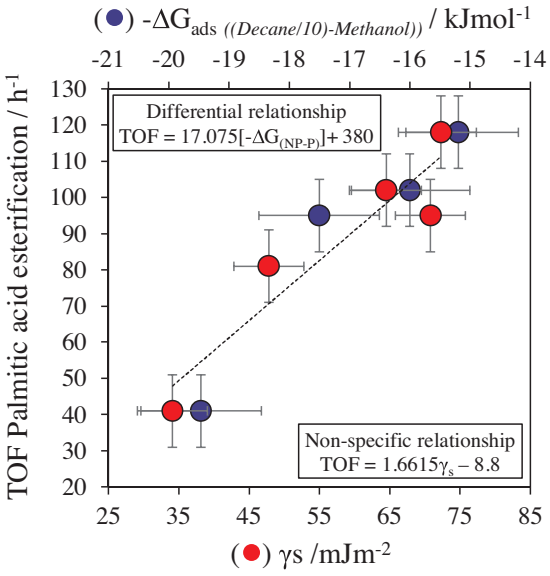

Fig. 6. Correlation of dispersive energy and $\left[-\Delta G^{C}_{NP-P}\right]$ for decane and methanol, with TOF for palmitic acid esterification with methanol.

organic content. These samples correspond to the E50 and B25 materials, respectively, and this non-linearity may reflect the different distributions, and associated adsorption characteristics, of ethyl versus phenyl framework moieties. BTSE, having only two carbon atoms, and similar molecular compatibility with TEOS, may be more uniformly distributed through the silica framework at lower loadings than the bulkier BTSB phenyl substituent. The different electronic properties of CH_2 versus CH substituents in ethyl versus phenyl functions may also impact upon surface adsorption. Calculations of the change in surface dispersive surface energy per C atom on introduction of BTSE or BTSB (Fig. S10) show that while γ_s per CH_2 site for E50 and E25 is the same, that for CH centres from phenyl groups in B50 and B25 is almost three times lower. This suggests that despite having a lower overall C content, ethyl groups are more effective in modifying the surface energy than phenyl moieties.

The relationship between catalytic esterification and surface chemistry was further explored by examining the difference in absolute (rather than extrapolated) free energies for adsorption of polar and non-polar probe molecules. The magnitude of non-specific dispersive interactions of hydrocarbon chains with a surface depends on chain length. In order to decouple non-specific and specific adsorption via polar and non-polar probe molecules, we hypothesised that the difference in adsorption free energies per carbon atom $-\Delta G^{C}_{NP-P}$ (Eqs. (5a) and (5b)) should be proportional to FFA adsorption and inversely proportional to water adsorption.

$$-\Delta G^{C}_{NP-P} = \frac{-\Delta G^{(C_nH_x)}_{ads}}{n - \left[-\Delta G^{MeOH}_{ads}\right]} \quad (5a)$$

$$-\Delta G^{C}_{NP-P} = \frac{RT \times \ln(V_{NP})}{n - RT \times \ln(V_P)} \quad (5b)$$

Values of $-\Delta G^{C}_{NP-P}$ calculated across the family of $PrSO_3H$-PMO catalysts are shown in Fig. S11, and are essentially independent of alkane chain length. Fig. 6 reveals a strong positive correlation between $-\Delta G^{C}_{Decane-MeOH}$ and γ^{D}_{S} with TOFs for palmitic acid esterification. Palmitic acid esterification is thus promoted as the adsorption of polar molecules such as methanol and water becomes disfavoured, and adsorption of the palmitic acid hydrocarbon backbone via non-specific dispersive interactions is enhanced. This finding is consistent with a Langmuir–Hinshelwood mechanism for esterification wherein methanol and FFA competitive adsorption is anticipated to dictate the rate of FAME production. Methanol-filled pores prevalent at high MeOH:FFA ratios will likely hinder FFA diffusion and adsorption within the hydrophilic pores of SBA-15, and hence slow esterification. In contrast, methanol binding to the more lipophilic PMO surfaces is significantly weakened relative to palmitic acid, and should facilitate a higher surface coverage and residence time for FFAs, and thus accelerate esterification. Reactively-formed water will desorb more rapidly from hydrophobic $PrSO_3H$-PMO catalysts, suppressing the (undesired) reverse hydrolysis reaction [71,79,80] which lowers FAME yields.

The direct correlation between TOF and $-\Delta G^{C}_{Decane-MeOH}$ and γ^{D}_{S} demonstrates that these parameters can be reliably used to predict the relative TOFs of sulfonated solid acid catalysts towards fatty acid esterification. Since $-\Delta G^{C}_{Decane-MeOH}$ requires only two adsorption measurements, this parameter offers a simple but powerful guide to the impact of hydrophobic surface modification upon catalyst activity without recourse to multiple alkanes necessary to calculate non-specific dispersive surface energy.

4. Conclusions

Periodic mesoporous organic SBA-15 materials have been synthesised with different concentrations of framework ethyl and phenyl bridging groups, offering porous solids with tunable surface energies and hydrophobicity. IGC was employed to measure the non-specific dispersive and specific surface energies for respective adsorption non-polar alkanes and polar oxygenates over hybrid organosilicas; non-specific dispersive surface energies rise steadily with the degree of organic functionalisation. Palmitic acid esterification with methanol was explored over sulfonated PMOs as a prototypical reaction that is sensitive towards water adsorption. $PrSO_3H$-PMOs with the highest non-specific dispersive energies exhibited the highest per site activity. Turnover Frequency in catalytic esterification is proportional to the difference in (chain length normalised) free energy of adsorption between non-polar and polar probe molecules $-\Delta G^{C}_{NP-P}$, offering a simple method to estimate surface hydrophobicity and its attendant impact on FAME production from free fatty acids.

Acknowledgements

We thank the EPSRC (EP/K000616/1, EP/F063423/1 and EP/G007594/3) for financial support and a Leadership Fellowship (AFL), and the Royal Society for the award of an Industry Fellowship (KW).

Please cite this article in press as: C. Pirez, et al., Can surface energy measurements predict the impact of catalyst hydrophobicity upon fatty acid esterification over sulfonic acid functionalised periodic mesoporous organosilicas? Catal. Today (2014), http://dx.doi.org/10.1016/j.cattod.2014.01.042

Appendix A. Supplementary data

Supplementary material related to this article can be found, in the online version, at http://dx.doi.org/10.1016/j.cattod.2014.01.042.

References

[1] J.H. Clark, Journal of Chemical Technology and Biotechnology 82 (2007) 603–609.
[2] F.R. Ma, M.A. Hanna, Bioresource Technology 70 (1999) 1–15.
[3] M. Canakci, J. Van Gerpen, Transactions of the ASAE 42 (1999) 1203–1210.
[4] M. Canakci, J. Van Gerpen, Transactions of the ASAE 44 (2001) 1429–1436.
[5] E. Lotero, Y.J. Liu, D.E. Lopez, K. Suwannakarn, D.A. Bruce, J.G. Goodwin, Industrial & Engineering Chemistry Research 44 (2005) 5353–5363.
[6] J. Dhainaut, J.-P. Dacquin, A.F. Lee, K. Wilson, Green Chemistry 12 (2010) 296–303.
[7] I.K. Mbaraka, D.R. Radu, V.S.Y. Lin, B.H. Shanks, Journal of Catalysis 219 (2003) 329–336.
[8] I.K. Mbaraka, B.H. Shanks, Journal of Catalysis 229 (2005) 365–373.
[9] I.K. Mbaraka, B.H. Shanks, Journal of Catalysis 244 (2006) 78–85.
[10] J.P. Dacquin, H.E. Cross, D.R. Brown, T. Duren, J.J. Williams, A.F. Lee, K. Wilson, Green Chemistry 12 (2010) 1383–1391.
[11] J.P. Dacquin, A.F. Lee, C. Pirez, K. Wilson, Chemical Communications 48 (2012) 212–214.
[12] C. Pirez, J.-M. Caderon, J.-P. Dacquin, A.F. Lee, K. Wilson, ACS Catalysis 2 (2012) 1607–1614.
[13] M.S. Cuevas, T.M. Deboni, P. Mielke Neto, F.S. Damasceno, R.V. Mota, L.H.M. da Silva, C.E.C. Rodrigues, A.J.A. Meirelles, Journal of the American Oil Chemists Society 90 (2013) 1589–1597.
[14] J.-Y. Park, D.-K. Kim, J.-S. Lee, Bioresource Technology 101 (2010) S62–S65.
[15] S.Z. Abidin, K.F. Haigh, B. Saha, Industrial & Engineering Chemistry Research 51 (2012) 14653–14664.
[16] C. Pirola, C.L. Bianchi, D.C. Boffito, G. Carvoli, V. Ragaini, Industrial & Engineering Chemistry Research 49 (2010) 4601–4606.
[17] D.E. Lopez, J.G. Goodwin, D.A. Bruce, E. Lotero, Applied Catalysis A: General 295 (2005) 97–105.
[18] K. Narasimharao, D.R. Brown, A.F. Lee, A.D. Newman, P.F. Siril, S.J. Tavener, K. Wilson, Journal of Catalysis 248 (2007) 226–234.
[19] L. Pesaresi, D.R. Brown, A.F. Lee, J.M. Montero, H. Williams, K. Wilson, Applied Catalysis A: General 360 (2009) 50–58.
[20] A. Alsalme, E.F. Kozhevnikova, I.V. Kozhevnikov, Applied Catalysis A: General 349 (2008) 170–176.
[21] K.N. Rao, A. Sridhar, A.F. Lee, S.J. Tavener, N.A. Young, K. Wilson, Green Chemistry 8 (2006) 790–797.
[22] D.E. Lopez, J.G. Goodwin Jr., D.A. Bruce, S. Furuta, Applied Catalysis A: General 339 (2008) 76–83.
[23] V.G. Deshmane, Y.G. Adewuyi, Applied Catalysis A: General 462 (2013) 196–206.
[24] M.L. Grecea, A.C. Dimian, S. Tanase, V. Subbiah, G. Rothenberg, Catalysis Science & Technology 2 (2012) 1500–1506.
[25] A. Patel, V. Brahmkhatri, N. Singh, Renewable Energy 51 (2013) 227–233.
[26] K. Saravanan, B. Tyagi, H.C. Bajaj, Catalysis Science & Technology 2 (2012) 2512–2520.
[27] Y. Liu, E. Lotero, J.G. Goodwin Jr., Journal of Catalysis 243 (2006) 221–228.
[28] T. Asefa, M.J. MacLachlan, N. Coombs, G.A. Ozin, Nature 402 (1999) 867–871.
[29] S. Inagaki, S. Guan, Y. Fukushima, T. Ohsuna, O. Terasaki, Journal of the American Chemical Society 121 (1999) 9611–9614.
[30] B.J. Melde, B.T. Holland, C.F. Blanford, A. Stein, Chemistry of Materials 11 (1999) 3302–3308.
[31] T. Asefa, M.J. MacLachlan, H. Grondey, N. Coombs, G.A. Ozin, Angewandte Chemie International Edition 39 (2000), 1808–+.
[32] S. Guan, S. Inagaki, T. Ohsuna, O. Terasaki, Journal of the American Chemical Society 122 (2000) 5660–5661.
[33] M.C. Burleigh, M.A. Markowitz, S. Jayasundera, M.S. Spector, C.W. Thomas, B.P. Gaber, Journal of Physical Chemistry B 107 (2003) 12628–12634.
[34] E.B. Cho, K. Char, Chemistry of Materials 16 (2004) 270–275.
[35] M.C. Burleigh, S. Jayasundera, C.W. Thomas, M.S. Spector, M.A. Markowitz, B.P. Gaber, Colloid and Polymer Science 282 (2004) 728–733.
[36] K. Nakajima, D.L. Lu, J.N. Kondo, I. Tomita, S. Inagaki, M. Hara, S. Hayashi, K. Domen, Chemistry Letters 32 (2003) 950–951.
[37] W.H. Wang, S.H. Xie, W.Z. Zhou, A. Sayari, Chemistry of Materials 16 (2004) 1756–1762.
[38] S. Inagaki, S. Guan, T. Ohsuna, O. Terasaki, Nature 416 (2002) 304–307.
[39] M.P. Kapoor, S. Inagaki, S. Ikeda, K. Kakiuchi, M. Suda, T. Shimada, Journal of the American Chemical Society 127 (2005) 8174–8178.
[40] A. Sayari, W.H. Wang, Journal of the American Chemical Society 127 (2005) 12194–12195.
[41] Q.H. Yang, M.P. Kapoor, S. Inagaki, Journal of the American Chemical Society 124 (2002) 9694–9695.
[42] C. Yoshina-Ishii, T. Asefa, N. Coombs, M.J. MacLachlan, G.A. Ozin, Chemical Communications (1999) 2539–2540.
[43] M.P. Kapoor, Q.H. Yang, S. Inagaki, Journal of the American Chemical Society 124 (2002) 15176–15177.
[44] K. Okamoto, Y. Goto, S. Inagaki, Journal of Materials Chemistry 15 (2005) 4136–4140.
[45] J. Morell, G. Wolter, M. Froba, Chemistry of Materials 17 (2005) 804–808.
[46] E.-B. Cho, D. Kim, Chemistry Letters 36 (2007) 118–119.
[47] M. Alvaro, M. Benitez, J.F. Cabeza, H. Garcia, A. Leyva, Journal of Physical Chemistry C 111 (2007) 7532–7538.
[48] Y. Goto, K. Nakajima, N. Mizoshita, M. Suda, N. Tanaka, T. Hasegawa, T. Shimada, T. Tani, S. Inagaki, Microporous and Mesoporous Materials 117 (2009) 535–540.
[49] Y. Goto, N. Mizoshita, O. Ohtani, T. Okada, T. Shimada, T. Tani, S. Inagaki, Chemistry of Materials 20 (2008) 4495–4498.
[50] K. Wilson, A.F. Lee, Catalysis Science & Technology 2 (2012) 884–897.
[51] A.A. Kiss, A.C. Dimian, G. Rothenberg, Advanced Synthesis & Catalysis 348 (2006) 75–81.
[52] J. Bico, U. Thiele, D. Quéré, Colloids and Surfaces A: Physicochemical and Engineering Aspects 206 (2002) 41–46.
[53] R.H. Mills, W.T.Y. Tze, D.J. Gardner, A. van Heiningen, Journal of Applied Polymer Science 109 (2008) 3519–3524.
[54] M.C. Almazan-Almazan, M. Perez-Mendoza, M. Domingo-Garcia, I. Fernandez-Morales, F. del Rey-Bueno, A. Garcia-Rodriguez, F.J. Lopez-Garzon, Carbon 45 (2007) 1777–1785.
[55] M.R. Cuervo, E. Asedegbega-Nieto, E. Diaz, S. Ordonez, A. Vega, A. Belen Dongil, I. Rodriguez-Ramos, Carbon 46 (2008) 2096–2106.
[56] F. Miano, Colloids and Surfaces A: Physicochemical and Engineering Aspects 110 (1996) 95–104.
[57] J.H. Xie, M. Bousmina, G.Y. Xu, S. Kaliaguine, Journal of Molecular Catalysis A: Chemical 135 (1998) 187–197.
[58] X. Zhang, L. Qian, P. Xu, H. He, Q. Du, Chemical Engineering Journal 137 (2008) 579–586.
[59] Y.-C. Yang, P.-R. Yoon, Materials Transactions 48 (2007) 1955–1960.
[60] Y.-C. Yang, P.-R. Yoon, Materials Transactions 48 (2007) 1548–1553.
[61] L. Qian, Y. Ren, T. Liu, D. Pan, H. Wang, G. Chen, Chemical Engineering Journal 213 (2012) 186–194.
[62] J.H. Xie, Q.L. Zhang, K.T. Chuang, Journal of Catalysis 191 (2000) 86–92.
[63] D. Gavril, B.E. Nieuwenhuys, Journal of Chromatography A 1045 (2004) 161–172.
[64] M.R. Cuervo, E. Diaz, B. de Rivas, R. Lopez-Fonseca, S. Ordonez, J.I. Gutierrez-Ortiz, Journal of Chromatography A 1216 (2009) 7873–7881.
[65] E. Diaz, S. Ordonez, A. Vega, A. Auroux, J. Coca, Applied Catalysis A: General 295 (2005) 106–115.
[66] B. Wang, W. Ran, Chemical Engineering Communications 199 (2012) 1236–1250.
[67] R. Sanchez-Vazquez, C. Pirez, J. Iglesias, K. Wilson, A.F. Lee, J.A. Melero, ChemCatChem 5 (2013) 994–1001.
[68] M.C. Gutierrez, J. Rubio, F. Rubio, J.L. Oteo, Journal of Chromatography A 845 (1999) 53–66.
[69] H.E. Newell, G. Buckton, D.A. Butler, F. Thielmann, D.R. Williams, Pharmaceutical Research 18 (2001) 662–666.
[70] D.Y. Zhao, Q.S. Huo, J.L. Feng, B.F. Chmelka, G.D. Stucky, Journal of the American Chemical Society 120 (1998) 6024–6036.
[71] P.L. Dhepe, M. Ohashi, S. Inagaki, M. Ichikawa, A. Fukuoka, Catalysis Letters 102 (2005) 163–169.
[72] Q.H. Yang, M.P. Kapoor, S. Inagaki, N. Shirokura, J.N. Kondo, K. Domen, Journal of Molecular Catalysis A: Chemical 230 (2005) 85–89.
[73] N. Hao, H. Wang, P.A. Webley, D. Zhao, Microporous and Mesoporous Materials 132 (2010) 543–551.
[74] J.B. Donnet, S.J. Park, H. Balard, Chromatographia 31 (1991) 434–440.
[75] F.M. Fowkes, Industrial & Engineering Chemistry 56 (1964) 40–52.
[76] Y. Peng, D.J. Gardner, Y. Han, Z. Cai, M.A. Tshabalala, Journal of Colloid and Interface Science 405 (2013) 85–95.
[77] A. Voelkel, Chemometrics and Intelligent Laboratory Systems 72 (2004) 205–207.
[78] G. Czeremuszkin, P. Mukhopadhyay, S. Sapieha, Journal of Colloid and Interface Science 194 (1997) 127–137.
[79] A. Karam, J.C. Alonso, T.I. Gerganova, P. Ferreira, N. Bion, J. Barrault, F. Jerome, Chemical Communications (2009) 7000–7002.
[80] G. Morales, G. Athens, B.F. Chmelka, R. van Grieken, J.A. Melero, Journal of Catalysis 254 (2008) 205–217.

Please cite this article in press as: C. Pirez, et al., Can surface energy measurements predict the impact of catalyst hydrophobicity upon fatty acid esterification over sulfonic acid functionalised periodic mesoporous organosilicas? Catal. Today (2014), http://dx.doi.org/10.1016/j.cattod.2014.01.042